ACS Combinatorial Science

Research Article

pubs.acs.org/acscombsci

Combinatorial Approach to Improve Photoelectrodes Based on $BiVO_4$

Chunping Jiang,[†,‡] Ruilin Wang,[†] and B. A. Parkinson*[,‡]

[†]College of Materials Science and Engineering, Sichuan University, Chengdu, Sichuan 610065, P.R. China

[‡]Department of Chemistry and School of Energy Resources, University of Wyoming, Laramie, Wyoming 82071, United States

ABSTRACT: The photoelectrochemical behavior of materials based on binary Bi−V oxides was investigated by preparing libraries of ternary metal oxides using high-throughput combinatorial inkjet printing of oxide precursors onto conductive glass substrates. Subsequent pyrolysis of the printed films, with addition of various levels of a third metal oxide precursor, produced libraries of metal oxides that were immersed under potential control into an electrolyte solution and evaluated for water photooxidation or photoreduction activity using a laser scanning technique to produce photocurrent images. It was found that the photoelectrolysis activity of the Bi−V oxides of various stoichiometries was best at a Bi/V ratio of 1 to 1 or the $BiVO_4$ phase. The photocurrent generation of this phase was improved by the addition of various amounts of W, Cu, Fe, Mg, and Mn. Addition of W led to the largest increase in photocurrent of up to 18 times; however the electronic band gap was increased compared to that of unsubstituted $BiVO_4$.

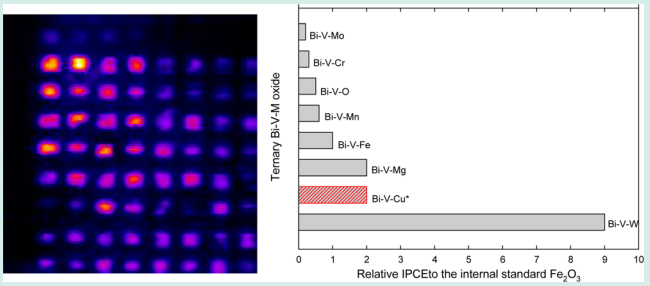

KEYWORDS: *water photoelectrolysis, semiconducting oxides, ink jet printing, laser scanning, photocurrent*

INTRODUCTION

The report of the photooxidation of water with rutile electrodes in 1972[1] set off a search for highly efficient, inexpensive, and stable water splitting photocatalysts. Many extensively investigated photocatalyst materials, such as TiO_2, only absorb UV light (E_g > 3.0 eV) which constitutes only 4% of the solar spectrum; therefore, suitable visible-light-driven materials need to be discovered and optimized.[2] $BiVO_4$, with a band gap of 2.4 eV, could be a promising photocatalyst material if used in a tandem photoelectrolysis cell with a lower bandgap semiconductor photoelectrode.[3,4] However, $BiVO_4$ till now has had rather poor photocurrent response resulting from inefficient separation and collection of photogenerated electron hole pairs.[5,6] Efforts to overcome these difficulties, such as the construction of a $WO_3/BiVO_4$ composite,[7] preparing a n-$BiVO_4$/p-Co_3O_4 heterojunction[8] and Eu or Ag addition to $BiVO_4$,[5,9,10] have resulted in only modest improvements in photoresponse. Some recent work, where the $BiVO_4$ films were electrodeposited[11] or produced by spray pyrolysis,[12] produced some substantial increases in photocurrent response. Other recent work includes alloying $BiVO_4$ with Mo or W[13−16] or depositing catalyst layers on the surface to enhance the photodriven oxygen evolution rate.[17−20] Theoretical work by Walsh et al.[21] on the electronic structure of $BiVO_4$, suggested that future work should consider adding nd^0 (including Ti^{4+}, V^{5+}, Mo^{6+}, W^{6+}, Zr^{4+}, Nb^{3+}, Ta^{5+}, Ce^{3+}, Pr^{3+}, and Nd^{3+}) and ns^2/nd^{10} cations (including Cu^{2+}, Zn^{2+}, Ga^{3+}, Ge^{4+}, Ag^{+}, Cd^{2+}, In^{3+}, Sn^{4+}, Bi^{3+}, and Pb^{2+}) to both reduce the oxide band gaps and increase the hole conductivity.[21] A very recent review has summarized the progress in $BiVO_4$ photoanodes for solar water oxidation.[22]

The band gap of $BiVO_4$ is too large for it to be highly efficient either by itself or in a tandem photoelectrolysis cell. Addition of other transition metals to the material may be able to lower its band gap to produce a potentially more efficient material. To efficiently produce and screen the many possible new oxide semiconductor compositions, combinatorial chemistry approaches need to be employed. Inkjet printing has played an important and increasing role in high-throughput combinatorial discovery and optimization of materials.[23−36] Our group has pioneered this combinatorial approach to identify and optimize the composition of visible-light-driven photocatalyst materials for water splitting.[37,38] Herein we extend this technique to quickly produce a diverse series of complex oxides based on Bi−V oxides. Recently Bard's group has also done a similar combinatorial study of photocatalysts related to $BiVO_4$ by using scanning electrochemical microscopy to study the photoactivity of libraries of Bi−V oxides with the addition of various third elements.[15] Herein we expand the number of compositions by using our ink jetting method to prepare ternary and quarternary Bi−V oxides by adding W, Mo, Mn, Co, Cr, Mg, Fe, or Cu and investigate their photoelectrolysis activity.

Received: September 25, 2012
Revised: July 31, 2013
Published: October 23, 2013

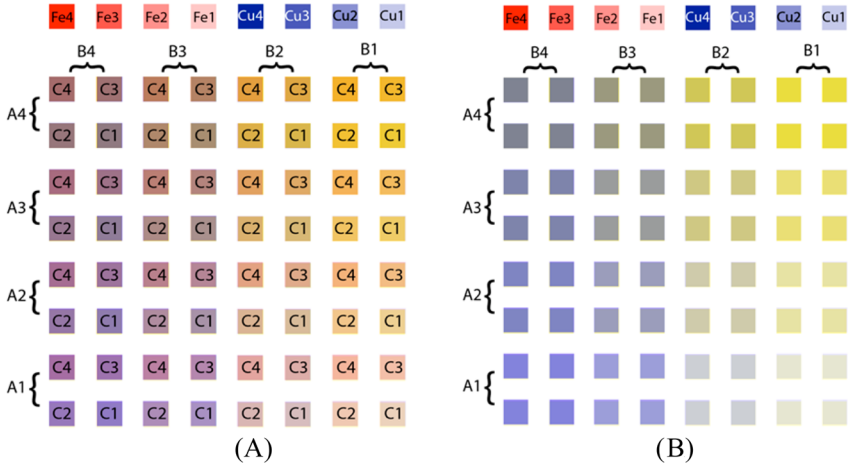

Figure 1. Printing templates used for optimizing the stoichiometry in all of the material systems. (A) Shows the scheme used for ternary mixtures. (B) Shows the template used for binary mixtures that produces groups of four squares with identical stoichiometries. The density of precursor drops (and the resulting stoichiometry) is shown in Table 1. The stoichiometries of the printed regions will be referred to using the values in column 4 of Table 1. For instance spot A2−B4−C3 in the template in Figure 1A would have a stoichiometry of $A_{1.7}B_{14.4}C_{3.7}$. Some squares such as $A_{14.4}B_{14.4}C_{14.4}$ (A4−B4−C4) and $A_{1.7}B_{1.7}C_{1.7}$ (A2−B2−C2) would have the same 1:1:1 stoichiometry but the A4−B4−C4 square would be about 8.5 times thicker than the A2−B2−C2 square (the thickness of the features on the diagonal increases from the bottom left to the upper right). Regions of Fe_2O_3 and CuO, as n and p type internal standards respectively, are prepared by printing four thicknesses of their precursors along the top row.

EXPERIMENTAL PROCEDURES

Materials. $Fe(NO_3)_3{\cdot}9H_2O$ and ammonium molybdate were obtained from Fisher Scientific. $Cu(NO)_3{\cdot}2.5H_2O$, $Co(NO_3)_2{\cdot}6H_2O$, $Bi(NO_3)_3{\cdot}5H_2O$, $Cr(NO_3)_3{\cdot}9H_2O$, $Mg(NO_3)_2$, $Mn(NO_3)_2{\cdot}xH_2O$ were all obtained from Alfa Aesar. Ammonium metatungstate hydrate and VCl_3 were obtained from Sigma Aldrich and Acros, respectively. All chemicals were used as received. Precut flourine-doped tin oxide (FTO) coated glass (TEC 8, 8-ΩR, 3.0 in. × 3.0 in.) was obtained from Pilkington Industries. The FTO glass was cleaned first by detergent, after rinsing with deionized water, then sonicated in the deionized water for 30 min, finally soaked in KOH solution and isopropyl alcohol for 24 h, and stored in methanol prior to printing. This procedure increased the hydrophilicity of the glass resulting in more uniform printing.

Preparation and Characterization of Combinatorial Printed Thin Film Libraries. All the material libraries were printed using a Dimatix model DMP-2800 piezoelectric ink jet printer. A formulation, suitable for the Dimatix inkjet printer, used solutions of the appropriate metal salts (0.3 M), except for ammonium molybdate (0.3 M) for which 8 drops of glycerol was added, with 35%, by volume, diethylene glycol and 1%, by volume, diethylene glycol monobutyl ether to serve the respective roles of viscosity agent and surfactant. $Bi(NO_3)_3$ was dissolved in 10% by volume solution of concentrated nitric acid in water. The solutions were then injected into empty Fujifilm Dimatix 1pL drop volume printer cartridges after a 10-min sonication. The following steps were similar to those reported by Woodhouse et al.[37] The stoichiometries of the various compositions were varied and controlled by both multiple printings of precursor and the variation of the precursor drop spacing. Often, to increase the thickness of the printed films, each metal precursor solution was overprinted up to 5 times because of the limited solubility of some of the metal precursors in the aqueous "inks". These 5 layer printed films had a thickness of about 30 nm as measured by cross sectional SEM images. The cartridges, because of their high acid content, were not stable for extended storage periods but were usable over several weeks of use before any corrosion of the copper contacts was apparent. When corrosion was apparent the cartridges were discarded. It is unlikely that the "inks" were exposed to copper since the corrosion was outside of the cartridges affecting only the contacts to the printer electronics.

A 9-row-by-8-column printing template, shown in Figure 1, was created with 3 mm × 3 mm individual squares spaced by 3 mm where in each square a predetermined amount of the metal salt precursors were printed.[38] The labels A, B, and C represent different metal oxide precursors. In the binary metal systems, only A and B are used; in ternary metal material systems, A, B, and C stand for the three different oxide precursors respectively whereas in the quarternary metal systems B stands for the Bi and V precursors printed at the same position from different cartridges, while A and C stand for the other two oxides precursors.

Table 1. Density of the Printed Precursor Drops Used to Produce the Mixtures Shown in Figure 1

label	drop spacing (μm)	drops per mm^2	relative stoichiometry
1	160	45	1.0
2	120	75	1.7
3	80	169	3.7
4	40	642	14.4

A series of printed libraries corresponding to the template above were then fired for 12 h at 500 °C in a ThermoLyne type 1300 furnace to decompose the precursors into metal oxides. The printed films were then connected as the working electrode to a Princeton Applied Research 174A potentiostat in an electrochemical cell containing a 0.1 M K_2SO_4 solution with a graphite rod acting as both the counter and the reference electrodes in a two-electrode configuration at biases ranging from −0.5 V (for the p-type materials) to 0.5 V (for the n-type materials). The custom built laser scanning station has selectable laser wavelengths of 405 nm (laser diode 40 mW), 473 nm (laser diode 35 mW), and 532 nm (frequency doubled CW-YAG 80 mW) but for most measurments λ = 405 nm was

dx.doi.org/10.1021/co300119q | ACS Comb. Sci. 2013, 15, 639−645

used. The laser power was measured with a Thorlabs PM 100 power meter and modulated with a mechanical chopper operating at 13 Hz. Note that the photocurrents for different experiments are not directly comparable because of variations in the laser power. Incident photocurrent efficiency (IPCE) values were calculated using the following equation:

$$\mathrm{IPCE}\%(\lambda) = 100 \times 1240 \times (J(\lambda)/\lambda I_0(\lambda)) \quad (1)$$

where λ is the wavelength, $J(\lambda)$ is the photocurrent (μA) under illumination at λ, and I_0 (λ) is the incident-light power (μW) at λ. The obtained IPCE vs position data was used to generate false color images of the IPCE values. False color images are useful for quick comparisons between the internal standard and the other oxides printed on the same FTO substrate. However, the actual IPCE values are needed to compare the photocatalytic activity of the different oxide compositions especially under different wavelengths of laser illumination. The majority of the prepared thin films are very thin with very small optical absorption and correspondingly low IPCE values. Very thin films are printed to minimize the need for carrier diffusion to produce photocurrent in these low mobility materials.

Larger-area thin films (2 cm × 2 cm) of specific compositions were prepared for SEM-EDS and X-ray diffraction (XRD) measurements to analyze their composition and structure. The XRD measurements were done either directly on the film at low angle or after scraping off some of the film and performing a conventional powder measurement using a SCINTAG XDS2000 automated powder diffraction system. The photoelectrochemical activity of these printed thin films were then investigated in a 3-electrode cell with a platinum wire, a saturated calomel electrode (SCE), and the thin film oxide electrode serving as the counter, reference, and working electrodes, respectively. Photocurrent measurements using various laser light sources were carried out in 0.1 M K_2SO_4 electrolyte that was nitrogen was purged 20 min prior to the experiments and then blanketed the electrolyte.

RESULTS AND DISCUSSION

Bi−V Binary Oxides. Since there are a number of known Bi−V oxides, such as $Bi_4V_2O_{11}$, $Bi_8V_2O_{17}$, $Bi_{25}VO_{40}$, we first investigated whether the usual stoichiometry of $BiVO_4$ was the optimum composition for the Bi−V binary oxide system.

The generic template used for binary Bi−V oxides, where B stands for Bi, and A stands for V is shown in Figure 1B. Figure 2 shows the false color IPCE map with a +0.5 V applied bias where the best n-type photoresponse spot corresponds to a Bi/V ratio of 14.4/14.4 or 1/1, as shown by the group of four features in the upper left of the image. There are three known crystal forms of $BiVO_4$, monoclinic sheelite, tetragonal zircon, and tetragonal scheelite. XRD was performed on a larger area film printed with a 1 to 1 Bi to V stoichiometry to determine which phase was produced from our precursors and firing conditions (Figure 3). The diffraction pattern shows peaks at 15.0°, 18.5°, 35.0°, and 46.0° corresponding the monoclinic scheelite phase of $BiVO_4$.[39] However, even the most photoactive square of Bi−V oxides has a 100 times lower photoactivity at 532 nm than at 405 nm since 532 nm light is very near the band gap of $BiVO_4$.

Bi−V−M Ternary Oxides. To attempt to improve the photocatalytic activity and spectral response of Bi−V oxides, a series containing a third metal (M), including Fe, Cu, Mn, Cr, Mg, W, and Mo, were prepared. Although we established that a 1:1 ratio of Bi and V has the best photoresponse for oxides

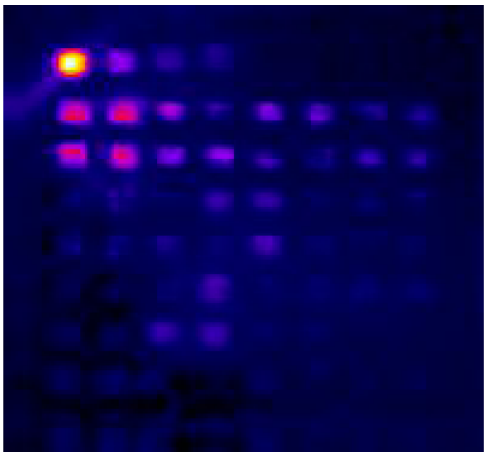

Figure 2. IPCE false color map of the binary Bi−V oxides with 405 nm laser illumination in 0.1 M K_2SO_4 solution with +0.5 V applied bias in a two-electrode cell.

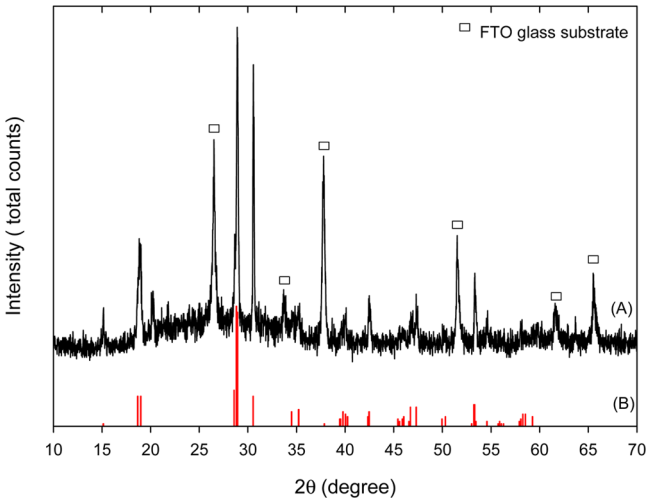

Figure 3. XRD pattern of (A) the thin film printed with the stoichiometry of Bi and V equal to 1 on the FTO glass and (B) monoclinic $BiVO_4$ (JCDPS 14-688).

containing only Bi and V, to investigate the ternary Bi−V−M oxides over a broad composition range, the template in Figure 1A was used where the ratio of Bi and V varied from 14.4:1 to 1:14.4. Figure 4 shows the IPCE values, for addition of the third metals listed above to a 1:1 Bi and V ratio, relative to the internal standard Fe_2O_3. All of the new materials showed n-type behavior with the exception of Bi−V−Cu oxides that are p-type. The introduction of tungsten brought about the most significant increase to the photocatalytic activity of Bi−V oxides whereas the addition of Mo or Cr decreased their photoresponse while Fe, Mn, Cu, and Mg resulted in only small improvements. The photocurrent of the best Bi−V−W combination under 405 nm illumination is 9 times more than that of the internal standard Fe_2O_3 and 18 times more than that of the binary $BiVO_4$. Bard et al. and others also identified the Bi−V−W oxides system as a promising combination.[13−16]

Since addition of W to the Bi−V combinations produced dramatic increases in IPCE values, further studies of this system were done. Three different laser wavelengths (405 nm, 473 nm, and 532 nm) were used to measure the wavelength dependence of the photoresponse of the Bi−V−W oxide library as shown in Figures 5A−C. It is apparent that (1) the addition of W

dx.doi.org/10.1021/co300119q | ACS Comb. Sci. 2013, 15, 639−645

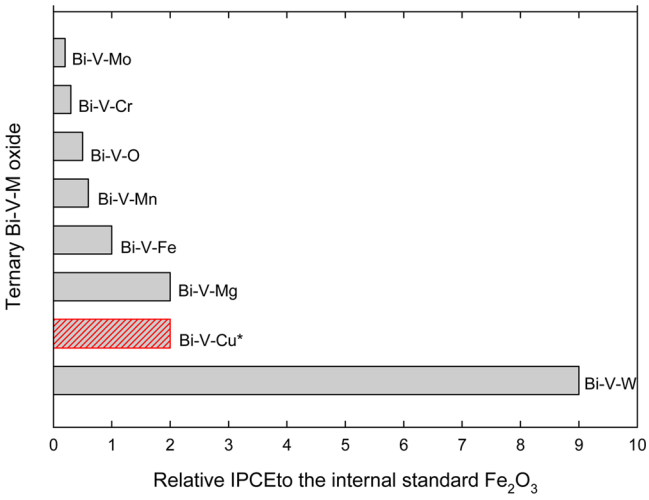

Figure 4. Relative IPCE at 405 nm of the best Bi–V combinations with the addition of a third metal with a +0.5 V applied bias in a two-electrode cell in in 0.1 M K_2SO_4 solution. The value of Bi–V–Cu oxide is relative to a CuO internal standard because it shows p-type photocatalytic activity and was scanned at a −0.5 V bias. Bi–V–O refers to $BiVO_4$ with no additional metals added. The best Bi–V–M metal ratios for the added metals were 3.7:3.7:1.7 for Mo, 3.7:14.4:1 for Cr, 14.4:14.4:3.7 for Mn, 14.4:14.4:3.7 for Fe, 14.4:14.4:1.7 for Mg, 1:1:14.4 for Cu, and 14.4:14.4:3.7 for W.

increased the photoresponse at 405 nm for most of Bi–V oxide combinations, (2) at 473 nm only W improved the photoresponse for the Bi–V oxides in which the ratio of Bi and V is larger than 1:1, and, (3) W did not increase the photoresponse of Bi–V oxides at 532 nm. Analysis of the three false color photocurrent images (Figures 5A–C) revealed that the largest photocurrent was located at the A4–B4–C3 square, correlating to the ratios $Bi_{14.4}V_{14.4}W_{3.7}$, and had a maximum IPCE of approximately 0.15%, about 10 times that of the internal standard Fe_2O_3 at 473 nm. (Note that that the stoichiometries reported herein only correspond to the printed ratios of the metal oxide precursors and the pyrolyzed films may contain multiple phases.) Another square with a similar stoichiometry, $Bi_{3.7}V_{3.7}W_{1.0}$ (A3–B3–C1), was also better than the Fe_2O_3 internal standard but not as high as the $Bi_{14.4}V_{14.4}W_{3.7}$ (A4–B4–C3) square. This is probably related to the different drop spacings resulting in the different thicknesses of the produced thin films. The most promising square was in Group #1, and to study this in detail squares from Group #1 to Group #4 on the diagonal in Figure 5A were chosen to further optimize of the composition and thickness. The template shown in Figure 1A was employed to make BiV–W oxides. In this pattern, Bi and V were printed 5 times at the same position of B separately, and then W was printed the same number of times at the position of A. Thus the squares from Group #1 to Group #4 in Figure 5A and 5D were comparable, and the same trend was observed in the photocurrents demonstrating the good reproducibility of

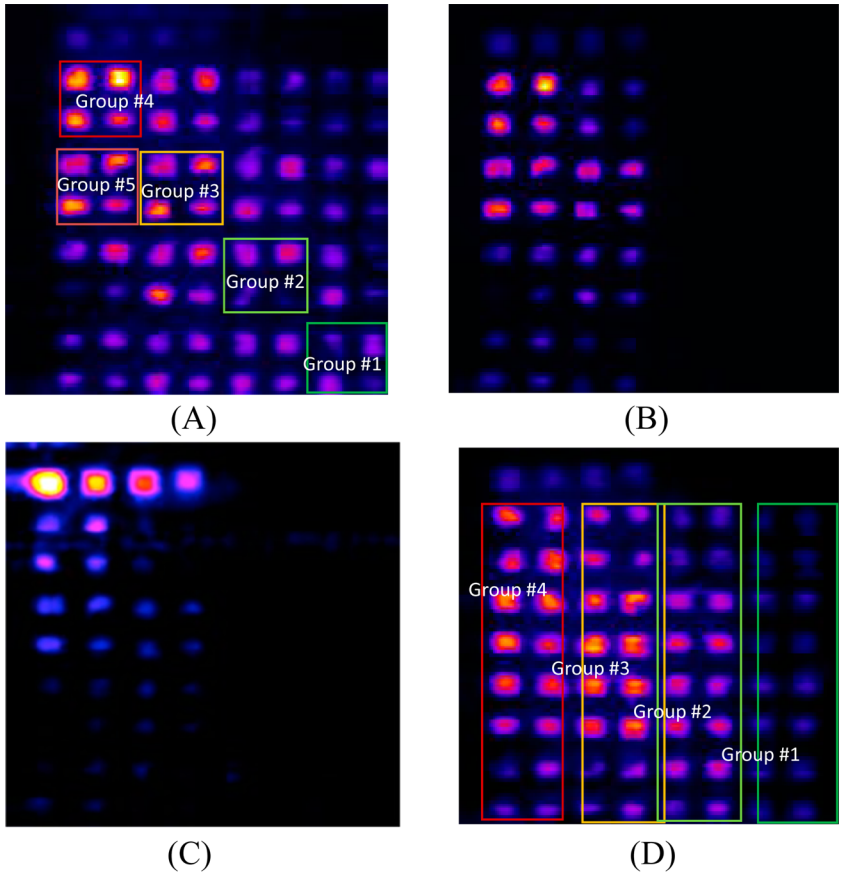

Figure 5. False color IPCE maps of compositional libraries of Bi–V–W prepared using the template from Figure 1A where A stands for V, B stands for Bi, and C stands for W with (A) 405 nm laser illumination, (B) 473 nm laser illumination, (C) 532 nm laser illumination with approximately the same photon flux. (D) False color IPCE map for BiV–W combinations using the template in Figure 1B where A stands for W, B stands for Bi and V printed one by one from different cartridges. All measurements were carried out in 0.1 M K_2SO_4 solution with +0.5 V applied bias.

dx.doi.org/10.1021/co300119q | ACS Comb. Sci. 2013, 15, 639–645

Table 2. Summary and Band Gaps and Maximum IPCE Values for 12 Larger-Area Samples Identified from Figure 5A

	group #4				group #3				group #5			
	$Bi_{14.4}V_{14.4}W_x$				Bi/V/W (3.7/3.7/x)				Bi/V/W (14.4/3.7/x)			
	A	B	C	D	E	F	G	H	I	J	K	L
x	1.0	1.7	3.7	14.4	1.0	1.7	3.7	14.4	1.0	1.7	3.7	14.4
W%[a]	3.4	5.6	11.4	33.3	11.9	18.7	33.3	66.1	5.2	8.6	17.0	44.3
E_g (eV)[b]	2.6	2.6	2.6	2.6	2.6	2.6	2.6	2.6	2.7	2.7	2.7	2.7
IPCE%[c]	1.8	2.2	2.1	1.3	0.9	0.35	0.9	0.7	0.1	0.4	0.1	0.2

[a]W% was the theoretical mole ratio of W in Bi−V−W oxides. [b]E_g (eV) band gap calculated from fitting the photocurrent spectra as in Figure 8. [c]IPCE%, was measured at 450 nm at 0.6 V in a two-electrode cell.

our inkjet printing method. Moreover, as was expected, the photocurrent of $Bi_{3.7}V_{3.7}W_{1.0}$ (A3−B3−C1) in Group #3 was improved, to be almost equal to the photocurrent of $Bi_{14.4}V_{14.4}W_{3.7}$ in Group #4 in Figure 5D, when the thickness was increased. However, it is still only half of the photocurrent of the $Bi_{14.4}V_{14.4}W_{3.7}$ (A4−B4−C3) square in Figure 5A. To further clarify the results, the 12 stoichiometries represented in the three groups of four in Figure 5A, showing the highest average photocurrent response, were chosen to more closely measure their properties.

Twelve larger-area thin films with compositions of the Groups 3−5 were prepared as shown in Table 2. Photocurrent−potential curves measured with 405 nm laser light chopped at 5 s intervals with a potential sweep rate of 5 mV/s with both front and back side illumination for the $Bi_{14.4}V_{14.4}W_{1.7}$ film are shown in Figure 8. The onset potential of the photocurrent is around −0.2 V providing an estimate of the flat band potential which in an n-type material is near the potential of conduction band. The band gap $Bi_{14.4}V_{14.4}W_{1.7}$ was measured to be around 2.6 eV making the potential of the valence band around 2.4 V (3.0 V vs NHE at pH = 0). Therefore the conduction band of this material appears to be lower than the potential for the reduction of H_2O whereas the valence band is more positive than the potential for O_2 evolution, indicating that this material can photooxidize water but cannot accomplish water splitting without an additional bias or another photoelectrode.

The inset of Figure 6 shows photocurrent versus time for slowly chopped illumination of a $Bi_{14.4}V_{14.4}W_{1.7}$ oxide electrode with 9.5 mW of 405 nm laser power. The calculated IPCE is around 8% at 0.5 V vs SCE. The bias for IPCE measurements in a two-electrode cell was set at 0.6 V. Sample B, $Bi_{14.4}V_{14.4}W_{1.7}$, is presented as an example. The IPCE spectra in 0.1 M K_2SO_4 solution are shown in spectra A and B of Figure 7. The IPCE of $BiVO_4$ was increased by about 10 times after addition of the appropriate amount of W. Because the printed film is so thin, we assume that the photocurrent, and subsequently the IPCE, is directly proportional to the absorption coefficient (α) for the material and that carrier diffusion length plays almost no role in the photocurrent since back illumination produces less photocurrent since most light is absorbed outside the space charge layer. Figure 6 shows that the photocurrent for a $Bi_{14.4}V_{14.4}W_{1.7}$ film is about twice as large from front side illumination than from backside illumination as would be expected from a short minority carrier diffusion length and most photocurrent arising from separation in the space charge layer. Since the thickness of the film measured in Figure 6 is only about 30 nm it is much thinner than the films fabricated to absorb much of the light.[17−20] Insight into carrier transport in a semiconducting thin film in a photoelectrochemical cell can often be obtained by comparison of the photocurrent obtained from front side and back side illumination. When illuminated from the front side, photoexcited electrons generated near the surface need to traverse

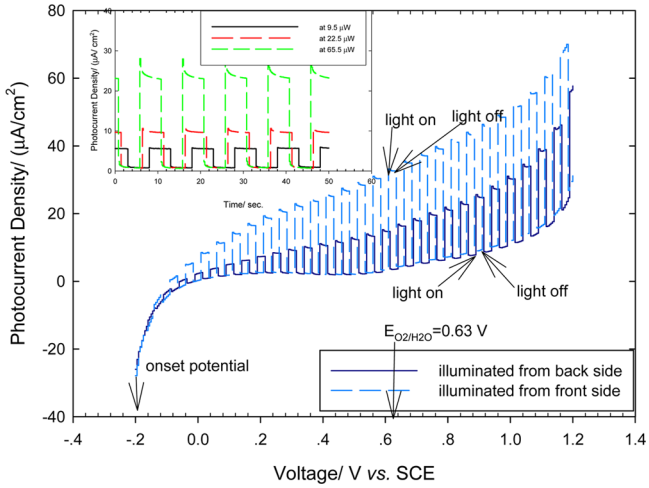

Figure 6. Current−potential curves for a $Bi_{14.4}V_{14.4}W_{1.7}$ oxide electrode under chopped illumination of 65.5 μW 405 nm laser in 0.1 M K_2SO_4. The solid dark blue curve is from back-side illumination while the dashed light blue curve is from front illumination. Inset is the corresponding photocurrent density-time curve at 0.5 V vs SCE in 0.1 M K_2SO_4 at different 405 nm laser powers.

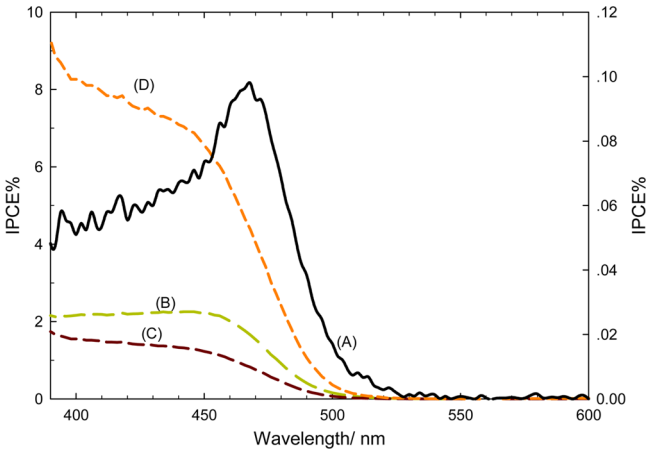

Figure 7. Wavelength dependence of IPCE for different printed samples. The right Y axis is for (A), the left Y axis is for (B), (C), and (D). Where (A) = $BiVO_4$ and (B) = $Bi_{14.4}V_{14.4}W_{1.7}$ are at 0.6 V in a two-electrode cell with 0.1 M K_2SO_4 solution in the AC method. (C) and (D) are $Bi_{14.4}V_{14.4}W_{1.7}$ at 0.5 V vs SCE in a three-electrode cell with 0.1 M K_2SO_4 solution in the AC and DC methods, respectively.

dx.doi.org/10.1021/co300119q | ACS Comb. Sci. 2013, 15, 639−645

the thickness of the thin film to the back contact whereas excited minority carrier holes, either generated in the space charge region or within the diffusion length of the space charge region, are more likely to reach the electrolyte interface to oxidize water. Back side illumination requires the minority carrier holes generated near the back contact to traverse the thickness of thin film, and fewer of them will be produced in the near surface space charge layer.

The band gap energy of $Bi_{14.4}V_{14.4}W_{3.7}$ was calculated by extrapolating the energy dependence of the photoreponse to the energy intercept. The indirect and direct transitions are around 2.6 eV, a little bigger than that of $BiVO_4$, as shown in Figures 8A and 8B. Using the same method, we measured the IPCE spectra and band gaps for 12 larger area samples of various compositions as shown in Table 2.

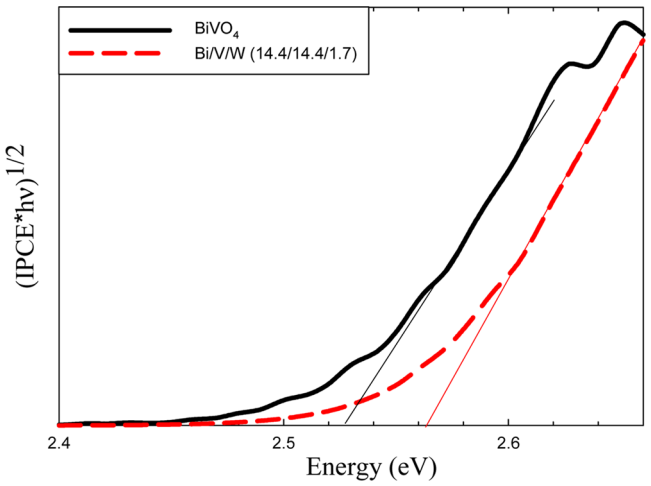

Figure 8. Linear extrapolation to approximate the band gap from the IPCE values fit to an indirect transition.

The samples were then analyzed to determine their phase composition. The SEM-EDS does not provide an accurate ratio of detected elements (Bi, V, W, and Sn from the substrate) because of the diverse composition in different areas is often a result of the spacing between the inkjetted drops. Combined with XRD, shown in Figure 9, some basic analysis of the composition could be done. In Group #3, only FTO peaks were found because the film was too thin. In Group #4 only $BiVO_4$ and FTO peaks were found for Samples A and B without any detectable WO_3. However a WO_3 peak was observed in Samples C and D indicating that the solubility limit of W in $BiVO_4$ had been exceeded and WO_3 and $BiVO_4$ phases coexist in these films. Considering the fact that the band gap of the phases that are present is 0.2 eV larger than that of $BiVO_4$ we can say that a small percentage of W is substituting for vanadium in the $BiVO_4$ structure which could act as an n-type dopant (W having one more electron than V) but also may be in high enough percentage to increase the band gap by 0.03 eV.

CONCLUSION

Inkjet printing was successfully employed to produce libraries of bismuth and vanadium containing metal oxide semiconductors to screen for improved photocatalytic properties compared with that of the parent Bi−V binary oxides. The best photoresponse was obtained from Bi−V−W semiconducting oxide, of nominal stoichiometry $Bi_{14.4}V_{14.4}W_{1.7}$, that is about 15 times of that of the $BiVO_4$ parent material at 450 nm. However,

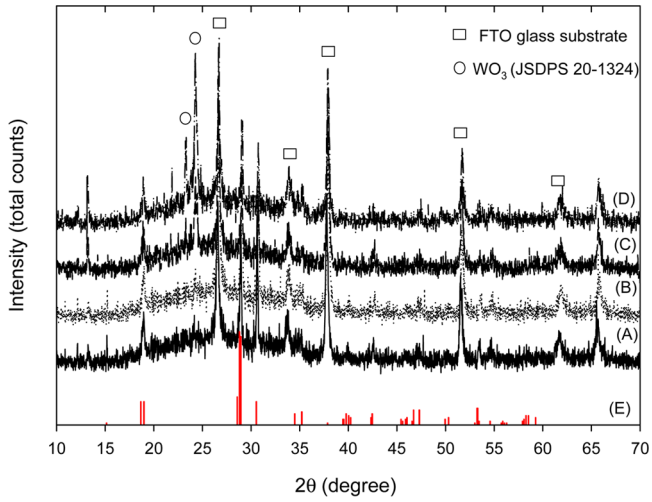

Figure 9. XRD pattern of (A) sample A, (B) sample B, (C) sample C, (D) sample D in Table 2, and (E) monoclinic $BiVO_4$ (JSDPS 14-688).

the band gap of the W containing phase was increased compared with that of the parent $BiVO_4$ phase, and the conduction band is still too low in energy to photoelectrolyze water into H_2 and O_2 without an applied bias or addition of a photocathode.

AUTHOR INFORMATION

Corresponding Author

*E-mail: bparkin1@uwyo.edu.

Funding

This work was supported by the NSF Funded Center for Chemical Innovation entitled Powering the Planet under Grant CHE-0802907. C.J. thanks the National Scholarship fund of China Scholarship Council for support.

Notes

The authors declare no competing financial interest.

REFERENCES

(1) Fujishima, A.; Honda, K. Electrochemical photolysis of water at a semiconductor electrode. *Nature* **1972**, *238* (5358), 37.

(2) Wang, D.; Zou, Z.; Ye, J. Photocatalytic O_2 evolution with the visible-light-driven photocatalysts $M_3V_2O_8$ (M = Mg, Zn). *Res. Chem. Intermed.* **2005**, *31* (4−6), 433−439.

(3) Kudo, A.; Omori, K.; Kato, H. A novel aqueous process for preparation of crystal form-controlled and highly crystalline $BiVO_4$ powder from layered vanadates at room temperature and its photocatalytic and photophysical properties. *J. Am. Chem. Soc.* **1999**, *121* (49), 11459−11467.

(4) Tokunaga, S.; Kato, H.; Kudo, A. Selective preparation of monoclinic and tetragonal $BiVO_4$ with scheelite structure and their photocatalytic properties. *Chem. Mater.* **2001**, *13* (12), 4624−4628.

(5) Kohtani, S.; Hiro, J.; Yamamoto, N.; Kudo, A.; Tokumura, K.; Nakagaki, R. Adsorptive and photocatalytic properties of Ag-loaded $BiVO_4$ on the degradation of 4-*n*-alkylphenols under visible light irradiation. *Catal. Commun.* **2005**, *6* (3), 185−189.

(6) Long, M.; Cai, W. M.; Cai, J.; Zhou, B. X.; Chai, X. Y.; Wu, Y. H. Efficient photocatalytic degradation of phenol over $Co_3O_4/BiVO_4$ composite under visible light irradiation. *J. Phys. Chem. B* **2006**, *110* (41), 20211−20216.

(7) Chatchai, P.; Murakami, Y.; Kishioka, S. Y.; Nosaka, A. Y.; Nosaka, Y. Efficient photocatalytic activity of water oxidation over $WO_3/BiVO_4$ composite under visible light irradiation. *Electrochim. Acta* **2009**, *54* (3), 1147−1152.

(8) Long, M. C.; Cai, W. M.; Kisch, H. Visible light induced photoelectrochemical properties of *n*-$BiVO_4$ and *n*-$BiVO_4$/*p*-Co_3O_4. *J. Phys. Chem. C* **2008**, *112* (2), 548−554.
(9) Zhang, A. P.; Zhang, J. Z. Effects of europium doping on the photocatalytic behavior of $BiVO_4$. *J. Hazard. Mater.* **2010**, *173* (1−3), 265−272.
(10) Zhang, A. P.; Zhang, J. Z. Synthesis and characterization of Ag/$BiVO_4$ composite photocatalyst. *Appl. Surf. Sci.* **2010**, *256* (10), 3224−3227.
(11) Dall'Antonia, L. H.; de Tacconi, N. R.; Chanmanee, W.; Timmaji, H.; Myung, N.; Rajeshwar, K. Electrosynthesis of bismuth vanadate photoelectrodes. *Electrochem. Solid State Lett.* **2010**, *13* (5), D29−D32.
(12) Liang, Y.; Tsubota, T.; Mooij, L. P. A.; van de Krol, R. Highly improved quantum efficiencies for thin film $BiVO_4$ photoanodes. *J. Phys. Chem. C* **2011**, *115* (35), 17594−17598.
(13) Berglund, S. P.; Rettie, A. J. E.; Hoang, S.; Mullins, C. B. Incorporation of Mo and W into nanostructured $BiVO_4$ films for efficient photoelectrochemical water oxidation. *Phys. Chem. Chem. Phys.* **2012**, *14*, 7065.
(14) Yao, W.; Iwai, H.; Ye, J. Effects of molybdenum substitution on the photocatalytic behavior of $BiVO_4$. *Dalton Trans.* **2008**, *11*, 1426.
(15) Park, H. S.; Kweon, K. E.; Ye, H.; Paek, E.; Hwang, G. S.; Bard, A. J. Factors in the Metal Doping of $BiVO_4$ for Improved Photoelectrocatalytic Activity as Studied by Scanning Electrochemical Microscopy and First-Principles Density-Functional Calculation. *J. Phys. Chem. C* **2011**, *115*, 17870−17879.
(16) Zhang, K.; Shin, X.-J.; Kim, J. K.; Park, J. H. Photoelectrochemical Cells with Tungsten Trioxide/Mo-Doped $BiVO_4$ Bilayers. *Phys. Chem. Chem. Phys.* **2012**, *14*, 11119−11124.
(17) Zhong, D. K.; Choi, S.; Gamelin, D. R. Near-Complete Suppression of Surface Recombination in Solar Photoelectrolysis by "Co-Pi" Catalyst-Modified W:$BiVO_4$. *J. Am. Chem. Soc.* **2011**, *133*, 18370.
(18) Abdi, F. F.; van de Krol, R. Thin Film Photoanodes Modified with Cobalt Phosphate Catalyst and W-doping. *J. Phys. Chem. C* **2012**, *116*, 9398.
(19) Seabold, J. A.; Choi, K.-S. Efficient and Stable Photo-Oxidation of Water by a Bismuth Vanadate Photoanode Coupled with an Iron Oxyhydroxide Oxygen Evolution Catalyst. *J. Am. Chem. Soc.* **2012**, *134*, 2186.
(20) Choi, S. K.; Choi, W.; Park, H. Solar Water Oxidation Using Nickel-Borate Coupled $BiVO_4$ Photoelectrodes. *Phys. Chem. Chem. Phys.* **2013**, *15*, 6499−6507.
(21) Walsh, A.; Yan, Y.; Huda, M. N.; Al-Jassim, M. M.; Wei, S. H. Band edge electronic structure of $BiVO_4$: Elucidating the role of the Bi s and V d orbitals. *Chem. Mater.* **2009**, *21* (3), 547−551.
(22) Park, Y.; McDonald, K. J.; Choi, K.-S. Progress in Bismuth Vanadate Photoanodes for Use in Solar Water Oxidation. *Chem. Soc. Rev.* **2013**, *42*, 2321−2337.
(23) Arrabito, G.; Musumeci, C.; Aiello, V.; Libertino, S.; Compagnini, G.; Pignataro, B. On the relationship between jetted inks and printed biopatterns: molecular-thin functional microarrays of glucose oxidase. *Langmuir* **2009**, *25* (11), 6312−6318.
(24) Calvert, P. Inkjet printing for materials and devices. *Chem. Mater.* **2001**, *13* (10), 3299−3305.
(25) Cheng, K.; Yang, M. H.; Chiu, W. W. W.; Huang, C. Y.; Chang, J.; Ying, T. F.; Yang, Y. Ink-jet printing, self-assembled polyelectrolytes, and electroless plating: Low cost fabrication of circuits on a flexible substrate at room temperature. *Macromol. Rapid Commun.* **2005**, *26* (4), 247−264.
(26) Hoth, C. N.; Schilinsky, P.; Choulis, S. A.; Brabec, C. J. Printing highly efficient organic solar cells. *Nano Lett.* **2008**, *8* (9), 2806−2813.
(27) Lennon, A. J.; Ho-Baillie, A. W. Y.; Wenham, S. R. Direct patterned etching of silicon dioxide and silicon nitride dielectric layers by inkjet printing. *Sol. Energy Mater. Sol. Cells* **2009**, *93* (10), 1865−1874.
(28) Lennon, A. J.; Utama, R. Y.; Lenio, M. A. T.; Ho-Baillie, A. W. Y.; Kuepper, N. B.; Wenham, S. R. Forming openings to semiconductor layers of silicon solar cells by inkjet printing. *Sol. Energy Mater. Sol. Cells* **2008**, *92* (11), 1410−1415.
(29) Marin, V.; Holder, E.; Wienk, M. M.; Tekin, E.; Kozodaev, D.; Schubert, U. S. Ink-jet printing of electron donor/acceptor blends: Towards bulk heterojunction solar cells. *Macromol. Rapid Commun.* **2005**, *26* (4), 319−324.
(30) Sanchez-Romaguera, V.; Madec, M. B.; Yeates, S. G. Inkjet printing of 3D metal-insulator-metal crossovers. *React. Funct. Polym.* **2008**, *68* (6), 1052−1058.
(31) Singh, M.; Haverinen, H. M.; Dhagat, P.; Jabbour, G. E. Inkjet printing-process and its applications. *Adv. Mater.* **2010**, *22* (6), 673−685.
(32) Small, A. C.; Johnston, J. H.; Clark, N. Inkjet printing of water "soluble" doped ZnS quantum dots. *Eur. J. Inorg. Chem.* **2010**, *2*, 242−247.
(33) Tseng, C. C.; Chang, C. P.; Sung, Y.; Chen, Y. C.; Ger, M. D. A novel method to produce Pd nanoparticle ink for ink-jet printing technology. *Colloids Surf., A* **2009**, *339* (1−3), 206−210.
(34) Wang, J.; Mohebi, M. M.; Evans, J. R. G. Two methods to generate multiple compositions in combinatorial ink-jet printing of ceramics. *Macromol. Rapid Commun.* **2005**, *26* (4), 304−309.
(35) Young, D.; Sukeshini, A. M.; Cummins, R.; Xiao, H.; Rottmayer, M.; Reitz, T. Ink-jet printing of electrolyte and anode functional layer for solid oxide fuel cells. *J. Power Sources* **2008**, *184* (1), 191−196.
(36) Teichler, A.; Eckardt, R.; Hoeppener, S.; Friebe, C.; Perelaer, J.; Senes, A.; Morana, M.; Brabec, C. J.; Schubert, U. S. Combinatorial Screening of Polymer:Fullerene blends for organic solar cells by inkjet printing. *Adv. Energy Mater.* **2011**, *1* (1), 105−114.
(37) Woodhouse, M.; Herman, G. S.; Parkinson, B. A. Combinatorial approach to identification of catalysts for the photoelectrolysis of water. *Chem. Mater.* **2005**, *17* (17), 4318−4324.
(38) Woodhouse, M.; Parkinson, B. A. Combinatorial discovery and optimization of a complex oxide with water photoelectrolysis activity. *Chem. Mater.* **2008**, *20* (7), 2495−2502.
(39) Sayama, K.; Nomura, A.; Arai, T.; Sugita, T.; Abe, R.; Yanagida, M.; Oi, T.; Iwasaki, Y.; Abe, Y.; Sugihara, H. Photoelectrochemical decomposition of water into H_2 and O_2 on porous $BiVO_4$ thin-film electrodes under visible light and significant effect of Ag ion treatment. *J. Phys. Chem. B* **2006**, *110* (23), 11352−11360.